Generation, Transformation, and Scattering of Long Waves Induced by a Short-Wave Group over Finite Topography

QINGPING ZOU*

Centre for Coastal Dynamics and Engineering, School of Marine Science and Engineering, University of Plymouth, Plymouth, United Kingdom

(Manuscript received 28 May 2010, in final form 23 March 2011)

ABSTRACT

Second-order analytical solutions are constructed for various long waves generated by a gravity wave train propagating over finite variable depth $h(x)$ using a multiphase Wentzel–Kramers–Brillouin (WKB) method. It is found that, along with the well-known long wave, locked to the envelope of the wave train and traveling at the group velocity C_g, a forced long wave and free long waves are induced by the depth variation in this region. The forced long wave depends on the depth derivatives h_x and h_{xx} and travels at C_g, whereas the free long waves depend on h, h_x, and h_{xx} and travel in the opposite directions at $\sqrt{gh}$. They interfere with each other and generate free long waves radiating away from this region. The author found that this topography-induced forced long wave is in quadrature with the short-wave group and that a secondary long-wave orbital velocity is generated by variable water depth, which is in quadrature with its horizontal bottom counterpart. Both these processes play an important role in the energy transfer between the short-wave groups and long waves. These behaviors were not revealed by previous studies on long waves induced by a wave group over finite topography, which calculated the total amplitude of long-wave components numerically without consideration of the phase of the long waves. The analytical solutions here also indicate that the discontinuity of h_x and h_{xx} at the topography junctions has a significant effect on the scattered long waves. The controlling factors for the amplitudes of these long waves are identified and the underlying physical processes systematically investigated in this presentation.

1. Introduction

As short-wave groups propagate toward the shore, second-order group bound long waves (often called infragravity waves, within the frequency band 0.004–0.04 Hz) can be induced by the quadratic difference interaction among pairs of primary waves. These long waves propagate with the wave envelope and evolve over variable water depth. They play an important role in many oceanographic and coastal problems such as harbor coastal structure resonance. Many efforts devoted to long waves have also been motivated by the fact that long waves may contribute more than a half of total wave energy in the nearshore region and therefore have significant impact on nearshore morphological change and shoreline evolution. Recent investigations of long waves have therefore been focusing on the generation, shoaling, and dissipation of long waves on a beach (Van Dongeren et al. 2003; Janssen et al. 2003; Battjes et al. 2004; Henderson et al. 2006).

Relatively less attention has been paid to long-wave dynamics in the intermediate water depth in the past decade. Theory on long waves at intermediate water depth was initiated by Munk (1949), Hasselmann et al. (1963), and Longuet-Higgins and Stewart (1962) and later verified against field observations by Tucker (1950), Elgar and Guza (1985), Okihiro et al. (1992), and Herbers et al. (1995). These studies assume constant water depth in an infinite domain. Finite topography such as sloping shelves, submarine canyons, and ridges are often found at intermediate water depth. A recent field study on the Southern California inner shelf however, showed that more than half of incident long-wave energy could be reflected by complex coastal bathymetry such as submarine canyons before entering beaches (Thomson et al.

* Current affiliation: Civil and Environmental Engineering, University of Maine, Orono, Maine.

Corresponding author address: Dr. Qingping Zou, Department of Civil and Environmental Engineering, University of Maine, Orono, ME 04469.
E-mail: qingping.zou@maine.edu

DOI: 10.1175/2011JPO4511.1

© 2011 American Meteorological Society

2006). Therefore, this study is concerned with the generation, transformation, and scattering of long waves when a short-wave group propagates over a finite variable water depth, which is intermediate relative to the wavelength of the short waves. Special attention is paid to the free long waves generated by the discontinuity of depth derivatives h_x and h_{xx} at the edge of the topography.

The envelope evolution of a gravity wave train for uniform depth has been extensively studied theoretically. Using a variational method, Whitham (1967, 1974) derived the modulation equations of hyperbolic/elliptic type for wave trains at a relative water depth kh smaller/larger than 1.36, indicating that wave trains are stable/unstable at these water depths. Hasimoto and Ono (1972) showed that the envelope evolution is governed by a nonlinear Schrodinger equation at lowest order and obtained the same instability criterion. Davey and Stewartson (1974) extended Hasimoto and Ono's results to two-dimensional (2D) wave packets, and Djordjevic and Redekopp (1977) extended Davey and Stewartson's formulation to include capillarity.

For variable bottom topography with a length scale of the same order as that of the envelope, Chu and Mei (1970) used a Wentzel–Kramers–Brillouin (WKB) technique to obtain a set of third-order wave modulation equations in conservation form, which includes higher-order derivatives than Whitham's. Mei and Benmoussa (1984) applied these equations at the second order to investigate the long waves induced by short-wave groups over an uneven bottom. Their numerical results indicate that, in addition to group bound long waves, new free long waves are generated and radiate away from the local topography at a shallow-water speed of $\sqrt{gh}$ at directions that may deviate from those of short-wave groups. Liu (1989) corrected Mei and Benmoussa's (1984) boundary conditions at the edge of the variable water depth and obtained the numerical results for a plane shelf that deviate from Mei and Benmoussa's (1984) considerably. We propose that the requirements of continuity of surface elevation and current at the edges of the finite topography are the physical interpretation of Liu's (1989) corrected matching conditions Unfortunately, Liu (1989) did not present any results for canyon and ridge, which are essential to our understanding of scattering of wave groups by complex topography. Over the finite topography, unlike Mei and Benmoussa (1984) and Liu (1989), who calculated the total amplitude of long waves numerically, we will construct the closed-form analytical solutions as a sum of 1) a forced long wave locked to the envelope of the wave train described by Longuet-Higgins and Stewart's (1962) solution for uniform water depth; 2) a topography-induced forced long wave bound to the wave group; and 3) two free long waves propagating at opposite directions. Over the constant water depth on the either side of the topography, we will obtain the analytical solutions for the transmitted and reflected free waves generated by and radiated away from the finite region of topography as indicated by Mei and Benmoussa's (1984) and Liu's (1989) numerical results.

The objective is to investigate the underlying physical processes controlling the topographical scattering of wave trains, the phase shift between these long-wave components and short-wave groups, and the associated energy transfer between them. We will also establish the general trend in amplitude variation of forced and free long waves over variable water depth and examine how the topographical scattering of a wave group is affected by the width and shape of topography and the discontinuity of depth derivatives h_x and h_{xx} at the edge of the topography in particular. In this presentation, we start with the same evolution equations as those of Mei and Benmoussa (1984) in section 2, derive the analytical solutions to wave evolution equations using a multiphase WKB method in section 3, apply the corrected boundary conditions in section 4, and then give some examples of analytical results for typical topography in section 5. Finally, in section 6, we conclude by summarizing the main findings in this study.

2. Governing equations

Following Whitham (1967), we take x and z as the horizontal and vertical coordinates, with $z = 0$ on the undisturbed free surface and $z = -h(x)$ on the bottom (see Fig. 1 for coordinate system and primary variables). We consider a train of slowly modulated, progressive waves over mild slope topography,

$$\varsigma^{(1)}(x,t) = \mathrm{Re}\left\{A(X,T)\exp\left[i\left(\int^x k\,dx - \omega t\right)\right]\right\}, \qquad (2.1)$$

where $\varsigma^{(1)}$ is the first-order free surface displacement associated with short waves, wavenumber k and wave frequency ω are $O(1)$ functions of the slowly varying coordinate $X = \varepsilon x$ and the slow time $T = \varepsilon t$, wave amplitude A is an $O(\varepsilon)$ function of X and T, $\varepsilon \ll 1$, and Re signifies the real part of the variable and will be omitted hereafter. For simplicity, we will focus on the normal incident wave groups over 1D bottom topography whose solutions can be readily adapted to 2D topography. A second-order long-wave component is induced by the short-wave group over a constant or variable water depth. The corresponding velocity potential and free surface displacement including short- and long-wave components are

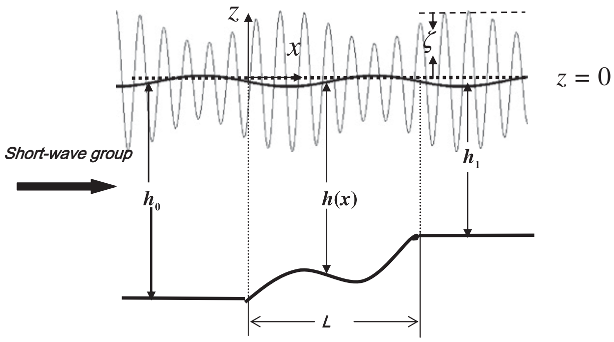

FIG. 1. Definition sketch of variables and coordinate system for a short-wave group propagating over a localized topography connecting with constant water depths.

$$\varphi = Ux - Pt - \frac{igA\cosh k(z+h)}{\omega\cosh kh}\exp\left[i\left(\int^x k\,dx - \omega t\right)\right]$$

and (2.2)

$$\varsigma(x,t) = \varsigma^{(1)} + \varsigma^{(2)}, \tag{2.3}$$

where $U(X, T)$ is the second-order short-wave-induced horizontal velocity, $P(X, T)$ is the second-order pressure, and $\varsigma^{(2)} = \eta(X, T)$ is the second-order short-wave-induced mean free surface displacement. Through the average Lagrangian method, we derive the following three equations with an error factor $1 + O(\varepsilon^2)$:

$$\frac{\partial}{\partial t}(E) + \frac{\partial}{\partial x}(C_g E) = 0, \tag{2.4a}$$

$$\frac{\partial \eta}{\partial t} + \frac{\partial}{\partial x}\left(Uh + \frac{E}{C}\right) = 0, \quad \text{and} \tag{2.4b}$$

$$\frac{\partial U}{\partial t} + \frac{\partial}{\partial x}\left(g\eta + \frac{C_g - C/2}{Ch}E\right) = 0, \tag{2.4c}$$

where

$$C = (gk^{-1}\tanh kh)^{1/2}, \tag{2.5a}$$

$$C_g = \frac{1}{2}C\left(1 + \frac{2kh}{\sinh 2kh}\right), \quad \text{and} \tag{2.5b}$$

$$E = \frac{1}{2}g[\mathrm{Re}(A)]^2 \tag{2.5c}$$

are the wave phase velocity, group velocity, and wave energy respectively (Zou 1995). Equations (2.4a)–(2.4c) represent wave action, mass, and momentum conservations, respectively, and are the same as Eqs. (2.6)–(2.8) of Mei and Benmoussa (1984). Cross-differentiating (2.4b) and (2.4c) to eliminate U, we have

$$\frac{\partial^2 \eta}{\partial t^2} - g\frac{\partial}{\partial x}\left(h\frac{\partial \eta}{\partial x}\right) = -\frac{\partial}{\partial x}\left[\frac{\partial}{\partial t}\left(\frac{E}{C}\right)\right] + \frac{\partial}{\partial x}\left[h\frac{\partial}{\partial x}\left(\frac{C_g - C/2}{Ch}E\right)\right], \tag{2.6}$$

which is equivalent to (2.9) in Mei and Benmoussa (1984), derived by Chu and Mei (1970). Substituting (2.4a) into governing Eq. (2.6) to eliminate $\partial(E/C)/\partial t$ gives

$$\frac{\partial}{\partial x}\left(gh\frac{\partial \eta}{\partial x}\right) - \frac{\partial^2 \eta}{\partial t^2} = -\frac{d^2 S}{dx^2}, \tag{2.7}$$

where $S = (2C_g/C - 1/2)E$ is the wave radiation stress. Equation (2.7) is the same as the governing equations (2.11) of Mei and Benmoussa (1984) and (7) of Janssen et al. (2003). In case of constant water depth, Eq. (2.7) becomes the wave setdown and setup equations for wave groups proposed by Longuet-Higgins and Stewart (1960, 1961, 1962) (Mei and Benmoussa 1984). We next obtain the analytical solution of (2.6) that satisfies proper boundary conditions at the topography edges.

3. Analytical solutions

In this section, the governing equations are solved for an incoming wave train of sinusoidal envelope

$$A(x,t) = a\exp\left[i\left(\int^x K\,dx - \Omega t\right)\Big/2\right], \tag{3.1a}$$

where

$$\Omega = \varepsilon\omega \quad \text{and} \tag{3.1b}$$

$$K(x) = \varepsilon\omega/C_g(x), \tag{3.1c}$$

traveling from a uniform depth h_0 in $x < 0$, through a region of variable depth $h(x)$ in $0 < x < L$, to a uniform depth h_1 in $x > L$ (cf. Fig. 1).

It follows from (2.5c) and (3.1a) that E may be decomposed into steady and oscillatory parts

$$E = \overline{E}(x) + \tilde{E}(x)\exp(-i\Omega t), \tag{3.2a}$$

where

$$\overline{E} = \frac{1}{4}\frac{C_{g0}}{C_g}ga_0^2, \tag{3.2b}$$

$$\tilde{E} = \frac{1}{4}\frac{C_{g0}}{C_g}ga_0^2\exp\left(i\int^x K\,dx\right), \tag{3.2c}$$

and a_0 and C_{g0} are the incident wave amplitude and group velocity in the incident side $x < 0$. According to (2.4b), (2.4c), and (3.2), η should take the form of E; that is,

$$\eta = \frac{1}{4} g C_{g0} a_0^2 [\overline{\eta}(x) + \tilde{\eta}(x)\exp(-i\Omega t)], \tag{3.3a}$$

where

$$\overline{\eta} = -\frac{C_g - C/2}{gC_g Ch} \tag{3.3b}$$

is the wave setdown. Combined with (3.2) and (3.3), (2.6) gives

$$\frac{d}{dx}\left(\frac{gh}{\Omega^2}\frac{d\tilde{\eta}}{dx}\right) + \tilde{\eta} = \left\{\frac{2C_g - C/2}{C_g^3 C} + (i\Omega)^{-1}\left[\frac{d}{dx}\left(\frac{2C_g - C/2}{C_g^2 C}\right) + \frac{h}{C_g}\frac{d}{dx}\left(\frac{C_g - C/2}{CC_g h}\right)\right] - \Omega^{-2}\frac{d}{dx}\left[h\frac{d}{dx}\left(\frac{C_g - C/2}{C_g Ch}\right)\right]\right\} \times \exp\left(i\int^x K\,dx\right). \tag{3.4}$$

We assume that the topography has a spatial scale of many wavelengths of the wave group; that is,

$$\frac{h_x}{\kappa h} = O(\mu), \tag{3.5a}$$

$$\frac{h_{xx}}{\kappa^2 h} = O(\mu^2), \ldots, \quad \text{and} \quad \mu \ll 1, \tag{3.5b}$$

so that the three terms on the right-hand side of (3.4) are $O(\mu^0)$, $O(\mu^1)$, and $O(\mu^2)$, respectively. We note that $h_x/Kh = O(\mu)$ is the same as the normalized bed slope β used by Battjes et al. (2004).

The solution of (3.4) is the sum of the particular solution corresponding to the forced wave $\tilde{\eta}_F$ and the homogeneous solutions corresponding to the forward and backward propagating free wave components $\tilde{\eta}_+$ and $\tilde{\eta}_-$; that is,

$$\tilde{\eta} = \tilde{\eta}_F + [\tilde{\eta}_+ + \tilde{\eta}_-]. \tag{3.6a}$$

We seek a particular solution of (3.4) corresponding to the forced wave through the asymptotic expansion of

$$\tilde{\eta}_F = \tilde{\eta}_F^{(0)} + \tilde{\eta}_F^{(1)} + \tilde{\eta}_F^{(2)} + \cdots = (\eta_F^{(0)} + \eta_F^{(1)} + \eta_F^{(2)} + \cdots)\exp\left(i\int_0^x K\,dx\right), \tag{3.6b}$$

where

$$\tilde{\eta}_F^{(n)}(x) = \eta_F^{(n)}(x)\exp\left(i\int_0^x K\,dx\right) = O(\mu^n) \quad (n = 0, 1, 2).$$

Substituting (3.6b) into (3.4), we obtain

$$\eta_F^{(0)}(x) = \frac{2C_g - C/2}{C_g^3 C(1 - gh/C_g^2)}, \tag{3.7a}$$

$$\eta_F^{(1)}(x) = \frac{(i\Omega)^{-1}}{(1 - gh/C_g^2)}\left\{\frac{d}{dx}\left(\frac{2C_g - C/2}{CC_g^2}\right) + \frac{h}{C_g}\frac{d}{dx}\left(\frac{C_g - C/2}{C_g Ch}\right) + g\left[\frac{2h}{C_g}\frac{d\eta_F^{(0)}}{dx} + \eta_F^{(0)}\frac{d}{dx}\left(\frac{h}{C_g}\right)\right]\right\}, \quad \text{and} \tag{3.7b}$$

$$\eta_F^{(2)}(x) = \frac{-\Omega^{-2}}{1 - gh/C_g^2}\left\{\frac{d}{dx}\left[h\frac{d}{dx}\left(\frac{C_g - C/2}{C_g Ch}\right)\right] + g\frac{d}{dx}\left(h\frac{d\eta_F^{(0)}}{dx}\right) + (i\Omega)g\left[\frac{2h}{C_g}\frac{d\eta_F^{(1)}}{dx} + \eta_F^{(1)}\frac{d}{dx}\left(\frac{h}{C_g}\right)\right]\right\}. \tag{3.7c}$$

Because $C(x) = C(k_\infty, h(x))$, $C_g(x) = (k_\infty, h(x))$, where $k_\infty = \omega^2/g$ is the deep-water wavenumber for the short wave, their gradients are given by

$$\frac{dC}{dx} = \frac{dC(k_\infty, h)}{dh}h_x, \quad \frac{dC_g}{dx} = \frac{dC_g(k_\infty, h)}{dh}h_x,$$

(3.7a) can be rewritten as

$$\eta_F^{(0)}(x) = \eta_F^{(0)}(k_\infty, h(x)), \tag{3.7d}$$

which depends on the local water depth monotonically. Therefore,

$$\frac{d\eta_F^{(0)}}{dx} = \frac{d\eta_F^{(0)}}{dh}h_x.$$

Similarly, (3.7b) can be rewritten as

$$\eta_F^{(1)}(x) = \frac{(i\Omega)^{-1}}{(1 - gh/C_g^2)}\left\{\frac{d}{dh}\left(\frac{2C_g - C/2}{CC_g^2}\right) + \frac{h}{C_g}\frac{d}{dh}\left(\frac{C_g - C/2}{C_g Ch}\right) + g\left[\frac{2h}{C_g}\frac{d\eta_F^{(0)}}{dh} + \eta_F^{(0)}\frac{d}{dh}\left(\frac{h}{C_g}\right)\right]\right\}h_x$$
$$= (i\Omega)^{-1}Q_F(k_\infty, h(x))h_x. \tag{3.7e}$$

Thus, $\eta_F^{(1)}(x)$ is linear in h_x and in quadrature with the forced wave solution $\eta_F^{(0)}(x)$ for constant water depth. Equation (3.7c) can be rewritten as

$$\eta_F^{(2)}(x) = \frac{-\Omega^{-2}}{1 - gh/C_g^2}\left\langle\left\{\frac{d}{dh}\left[h\frac{d}{dh}\left(\frac{C_g - C/2}{C_g Ch}\right)\right] + g\frac{d}{dh}\left(h\frac{d\eta_F^{(0)}}{dh}\right) + g\frac{2h}{C_g}\frac{dQ_F}{dh} + Q_F\frac{d}{dh}\left(\frac{h}{C_g}\right)\right\}h_x^2 + \left[h\frac{d}{dh}\left(\frac{C_g - C/2}{C_g Ch}\right) + gh\frac{d\eta_F^{(0)}}{dh} + g\frac{2h}{C_g}Q_F\right]h_{xx}\right\rangle \tag{3.7f}$$

where $\eta_F^{(2)}(x)$ is proportional to h_x^2 and h_{xx} and in phase with the forced wave solution $\eta_F^{(0)}(x)$ for constant water depth.

Following a similar procedure, we obtain the homogeneous solution of Eq. (3.4), which corresponds to free wave components. Over the constant water depth regions, free waves must propagate away from the zone of variable depth $0 < x < L$; therefore, the homogeneous solution is the sum of two free waves traveling at opposite directions, $\tilde{\eta}_+$ and $\tilde{\eta}_-$,

$$\tilde{\eta}_+(x) = \begin{cases} 0 & (x<0) \\ C_+[\eta_+^{(0)} + \eta_+^{(1)}]\exp\left(i\int_0^x K_h\,dx\right) & (0<x<L) \quad \text{and} \\ T\eta_+^{(0)}\exp\left(i\int_0^x K_h\,dx\right) & (x>L) \end{cases} \tag{3.8a}$$

$$\tilde{\eta}_-(x) = \begin{cases} R\eta_-^{(0)}\exp\left(-i\int_0^x K_h\,dx\right) & (x<0) \\ C_-[\eta_-^{(0)} + \eta_-^{(1)}]\exp\left(-i\int_0^x K_h\,dx\right) & (0<x<L), \\ 0 & (x>L) \end{cases} \tag{3.8b}$$

where the plus and minus subscripts symbolize the amplitudes of the free waves propagating in the positive and negative x directions, $K_h(x) = \Omega/\sqrt{gh}$ is the wavenumber for free waves, and $\Omega/K_h = \sqrt{gh}$ is the magnitude of propagating speed of free waves. Here, $\eta_\pm^{(n)} = O(\mu^n)$ $(n = 0, 1)$, and C_+, C_-, R, and T are four complex coefficients determined by the four boundary conditions at $x = 0$ and $x = L$, which are given in the next section.

The asymptotic expansion of the homogeneous part of the Eq. (3.4) gives

$$\frac{2h}{\sqrt{gh}}\frac{d\eta_\pm^{(0)}}{dx} + \eta_\pm^{(0)}\frac{d}{dx}\left(\frac{h}{\sqrt{gh}}\right) = 0 \quad \text{and} \tag{3.9a}$$

$$\frac{d}{dx}\left(h\frac{d\eta_\pm^{(0)}}{dx}\right) \pm (i\Omega)\left[\frac{2h}{\sqrt{gh}}\frac{d\eta_\pm^{(1)}}{dx} + \eta_\pm^{(1)}\frac{d}{dx}\left(\frac{h}{\sqrt{gh}}\right)\right] = 0, \tag{3.9b}$$

The solution for (3.9a) is given by

$$\eta_\pm^{(0)}(x) = (i\Omega)^{-1}h^{-1/4}. \tag{3.9c}$$

Substituting (3.9c) into (3.9b), we obtain

$$\eta_\pm^{(1)}(x) = \pm\frac{1}{2}\Omega^{-2}g^{1/2}h^{-1/4}\int_0^x h^{-1/4}\frac{d}{dx}\left[h\frac{d}{dx}(h^{-1/4})\right]dx. \tag{3.9d}$$

According to (3.3a), the transient solution to Eq. (2.6) is therefore the sum of two superimposed components on the incident and transmission sides of the variable water depth and four superimposed components over the variable water depth,

$$\tilde{\eta} = \begin{cases} \tilde{\eta}_F^{(0)} + \tilde{\eta}_- & (x<0) \\ \tilde{\eta}_F^{(0)} + [\tilde{\eta}_F^{(1)} + \tilde{\eta}_F^{(2)}] + \tilde{\eta}_+ + \tilde{\eta}_- & (0<x<L), \\ \eta_F^{(0)} + \tilde{\eta}_+ & (x>L) \end{cases} \tag{3.10a}$$

where

$$\tilde{\eta}_F^{(0)}(x) = \eta_F^{(0)}\exp\left(i\int_0^x K\,dx\right) \tag{3.10b}$$

is the forced long-wave component locked to the envelope of the wave train, equivalent to Longuet-Higgins and Stewart's (1964) long-wave solution for uniform water depth;

$$[\tilde{\eta}_F^{(1)} + \tilde{\eta}_F^{(2)}] = [\eta_F^{(1)} + \eta_F^{(2)}]\exp\left(i\int_0^x K\,dx\right) \tag{3.10c}$$

is the change in the forced long-wave solution induced by variable water depth, propagating at the wave-group speed C_g; and $\tilde{\eta}_+$ and $\tilde{\eta}_-$ are the forward and backward propagating free gravity wave defined by (3.9), which radiate away from the local topography at a shallow-water wave-group speed $\sqrt{gh}$.

4. Boundary conditions

According to (2.4c), (3.2) and (3.3), U relates to η by

$$\frac{\partial U}{\partial t} = -\frac{\partial}{\partial x}\left(g\eta + \frac{C_g - C/2}{Ch}E\right) = -\frac{\partial}{\partial x}(g\eta_E),$$

where

$$\eta_E = \eta + \frac{C_g - C/2}{gCh}E$$

is the effective surface elevation whose complex amplitude is $\tilde{\eta}_E = \tilde{\eta} - \overline{\eta}\exp(i\int_0^x K\,dx)$. The boundary conditions follow from the requirement of continuity of surface elevation η and current U at the topography edges $x = 0$ and $x = L$; that is,

$$\tilde{\eta}(0^+) = \tilde{\eta}(0^-), \tag{4.1a}$$

$$\tilde{\eta}(L^+) = \tilde{\eta}(L^-), \tag{4.1b}$$

$$\frac{d\tilde{\eta}_E(0^+)}{dx} = \frac{d\tilde{\eta}_E(0^-)}{dx}, \quad \text{and} \tag{4.1c}$$

$$\frac{d\tilde{\eta}_E(L^+)}{dx} = \frac{d\tilde{\eta}_E(L^-)}{dx}. \tag{4.1d}$$

Boundary conditions (4.1a) and (4.1b) are the same as those of Mei and Benmoussa (1984) and Liu (1989), whereas (4.1c) and (4.1d) are different from those of Mei and Benmoussa (1984) but identical to those of Liu (1989). Liu derived the latter boundary conditions by integrating the governing equation of η equivalent to (3.4) from $x = x_0 - \delta$ to $x_0 + \delta$ ($x_0 = 0, L$) and taking the limit as $\delta \to 0$. Substituting (3.10a) into (4.1a) and (4.1b) and considering that $\tilde{\eta}_F^{(0)}$ is continuous across the topography edges $x = 0$ and $x = L$, we have

$$\tilde{\eta}_-(0^-) = [\tilde{\eta}_F^{(1)}(0^+) + \tilde{\eta}_F^{(2)}(0^+)] + \tilde{\eta}_+(0^+) + \tilde{\eta}_-(0^+) \quad \text{and} \tag{4.1e}$$

$$\tilde{\eta}_+(L^+) = [\tilde{\eta}_F^{(1)}(L^-) + \tilde{\eta}_F^{(2)}(L^-)] + \tilde{\eta}_+(L^-) + \tilde{\eta}_-(L^-), \tag{4.1f}$$

which implies that the reflected free wave is equal to the topography-induced forced + free waves $[\tilde{\eta}_F^{(1)} + \tilde{\eta}_F^{(2)}] + \tilde{\eta}_+ + \tilde{\eta}_-$ at the incident edge of the topography and that the transmitted free wave is equal to $[\tilde{\eta}_F^{(1)} + \tilde{\eta}_F^{(2)}] + \tilde{\eta}_+ + \tilde{\eta}_-$ at the transmission edge of the topography.

Substituting (3.7)–(3.10) and (3.3b) into (4.1), we derived T and R to the second order as shown in Eqs. (A3) and (A4) in the appendix. To elucidate the mechanisms contributing to topographical scattering and generation of long waves, we only show the first-order approximation of T and R here,

$$C_+ = -\frac{1}{2}\left[\left(1 + \sqrt{gh_0}/C_{g0}\right)Q_{10}(0^+) + \sqrt{gh_0}Q_{00}(0^+)/C_{g0}\right] + O(h_x^2, h_{xx}), \tag{4.2a}$$

$$C_- = -\frac{1}{2}\left[\left(1 - \sqrt{gh_1}/C_{g1}\right)Q_{10}(L^-) - \sqrt{gh_1}Q_{00}(L^-)/C_{g1}\right] \times \exp\left[i\int_{0^+}^{L^-}(K + K_h)\,dx\right] + O(h_x^2, h_{xx}), \tag{4.2b}$$

$$T = -\frac{1}{2}\left\{\left[\left(1 + \sqrt{gh_0}/C_{g0}\right)Q_{10}(0^+) + \sqrt{gh_0}Q_{00}(0^+)/C_{g0}\right] - \left[\left(1 + \sqrt{gh_1}/C_{g1}\right)Q_{10}(L^-) + \sqrt{gh_1}Q_{00}(L^-)/C_{g1}\right] \times \exp\left[i\int_{0^+}^{L^-}(K - K_h)\,dx\right]\right\} + O(h_x^2, h_{xx}), \quad \text{and} \tag{4.3a}$$

$$R = \frac{1}{2}\left\{\left[\left(1 - \sqrt{gh_0}/C_{g0}\right)Q_{10}(0^+) - \sqrt{gh_0}Q_{00}(0^+)/C_{g0}\right] - \left[\left(1 - \sqrt{gh_1}/C_{g1}\right)Q_{10}(L^-) - \sqrt{gh_1}Q_{00}(L^-)/C_{g1}\right] \times \exp\left[i\int_{0^+}^{L^-}(K + K_h)\,dx\right]\right\} + O(h_x^2, h_{xx}), \tag{4.3b}$$

where

$$Q_{10}(x) = \eta_F^{(1)}/\eta_+^{(0)} = Q_F(k_\infty, h)h^{1/4}h_x \quad \text{and} \tag{4.4a}$$

$$Q_{00}(x) = (i\Omega)^{-1}C_g\eta_{Ex}^{(0)}/\eta_+^{(0)} = C_g h^{1/4}\left[\frac{d\eta_F^{(0)}(k_\infty, h)}{dh} - \frac{d\overline{\eta}(k_\infty, h)}{dh}\right]h_x. \tag{4.4b}$$

The quantity $Q_F(k_\infty, h)$ is defined by (3.7e); h_0, C_{g0} and h_1, C_{g1} are the values taken by h and C_g in the constant water depth regions $x < 0$ and $x > L$; subscript x denotes the x derivative; and $\eta_E^{(0)} = \eta_F^{(0)} - \overline{\eta}$. According to (4.4),

Q_{10} and Q_{00} are proportional to bottom slope h_x. Thus, according to (4.3), T and R are proportional to Q_{10} and Q_{00} at $x = 0+$ and $L-$ and therefore to the discontinuity of bottom slope h_x at the incident and transmit edge of the topography, with an oscillatory coefficient $\exp[i\int_{0^+}^{L^-}(K + K_h)\,dx]$ due to interference of free and forced waves with wavenumbers of K and K_h. Because the bottom slope before and after the topography is zero, when bottom slope h_x is continuous at the edge of the topography [i.e., $h_x(0^+) = h_x(0^-) = 0$ and $h_x(L^-) = h_x(L^+) = 0$], we have $Q_{00}(0^+) = Q_{00}(L^-) = 0$ and $Q_{10}(0^+) = Q_{10}(L^-) = 0$; thus $T = R = 0$ at the first order. In these cases, as shown by the higher-order expression of T and R given by Eqs. (A3) and (A4) in the appendix, the amplitude of reflected and transmitted waves are then dependent on the second-order depth gradient h_{xx} at the incident and transmit edge of the topography.

According to (4.3) and (4.4), the amplitudes of reflected and transmitted waves, given by $R\tilde{\eta}_-^{(0)}$ and $T\tilde{\eta}_+^{(0)}$, are proportional to $\eta_F^{(1)}$ and $\eta_{Ex}^{(0)}$ at the edge of the topography, which are proportional to the bottom slope h_x and inversely proportional to $(1 - gh/C_g^2)$ according to (3.7), so that the reflected and transmitted waves decrease with the relative water depth $k_\infty h$. According to (3.8) and (3.10), the long wave within the zone of variable depth $0 \le x \le L$ comprises four components: $\tilde{\eta}_F^{(0)}$, $[\tilde{\eta}_F^{(1)} + \tilde{\eta}_F^{(2)}]$, $\tilde{\eta}_+$, and $\tilde{\eta}_-$. The first two are group bound and propagate in the same direction as the wave envelope and short waves themselves at the speed of C_g, whereas the last two are free gravity waves traveling in the same and opposite direction to wave groups at the speed of $\sqrt{gh}$. The last three waves interfere with each other and generate a reflected free wave at $x = 0$ and a transmitted free wave at $x = L$ [cf. (3.10) with (4.1a) and (4.1b)]. According to (4.3), the transmitted and reflected free waves include a slowly varying amplitude that depends on h_x and h_{xx} at the junctions and fast varying phases $\exp[i\int_{0^+}^{L^-}(K - K_h)\,dx]$ and $\exp[i\int_{0^+}^{L^-}(K + K_h)\,dx]$. According to (4.3), the reflected wave amplitude $R\tilde{\eta}_-^{(0)}$ attains local minimum and maximum at $x = 0$, when $\int_{0^+}^{L^-}(K + K_h)\,dx = \int_{0^+}^{L^-}\Omega[(gh)^{1/2} + C_g]\,dx = (n + 1/2)\pi$ and $n\pi$, respectively, and the transmitted wave $T\tilde{\eta}_+^{(0)}$ attains its minimum and maximum at $x = L$, when $\int_{0^+}^{L^-}(K - K_h)\,dx = \int_{0^+}^{L^-}\Omega[(gh)^{1/2} - C_g]\,dx = (n + 1/2)\pi$ and $n\pi$, respectively. For a fixed depth function $h(x)$ and changing L, the amplitudes of radiating waves oscillate around a value that depends on the discontinuities of h_x and h_{xx} at the junctions. This behavior is similar to those of gravity waves over a ramp predicted by Miles and Zou (1992) and over a trench by Kirby and Dalrymple (1983).

5. Energy transfer to long waves

Assuming steady state and negligible dissipation, the energy balance of long waves is largely determined by the energy transfer from the short-wave groups to long waves, which can be described by (Battjes et al. 2004; Phillips 1977)

$$W = -\left\langle U_{\text{total}}\frac{dS}{dx}\right\rangle, \tag{5.1}$$

where $U_{\text{total}} = U + E/(Ch)$ is the total long-wave currents including the mass flux of the primary wave $E/(Ch)$, $\langle\,\rangle$ is time average, and $S = (2C_g/C - 1/2)E$ is the short-wave radiation stress.

Substituting (3.3a) and (3.10) into (2.4b), we obtain the complex amplitude of U_{total},

$$\begin{aligned}\tilde{U}_{\text{total}}(x) = \frac{1}{4}gC_{g0}a_0^2\Bigg\{&\left[\frac{C_g}{h}(\eta_F^{(0)} + \eta_F^{(1)} + \eta_F^{(2)})\right]\exp\left(i\int_0^x K\,dx\right) + \frac{\sqrt{gh}}{h}\left[\eta_+\exp\left(i\int_0^x K_h\,dx\right) - \eta_-\exp\left(-i\int_0^x K_h\,dx\right)\right]\\ &-\left[\frac{C_g}{i\Omega h}\frac{d}{dx}(C_g\eta_F^{(0)})\right]\exp\left(i\int_0^x K\,dx\right)\Bigg\},\end{aligned} \tag{5.2}$$

where η_+ and η_- are the amplitudes of forward and backward propagating free waves [cf. (3.8)]. The first and second square brackets of (5.2) are the currents induced by the long waves that satisfy the relationship of $U = C_g\varsigma/h$. The third square bracket is the current induced by topographical changes and mass conservation requirement. Here,

$$\tilde{S} = \frac{1}{4}gC_{g0}a_0^2\left(\frac{2C_g - C/2}{CC_g}\right)\exp\left(i\int_0^x K\,dx\right)$$

is the complex amplitude of shortwave radiation stress. The complex amplitude of the gradient of wave radiation stress is therefore given by

$$\begin{aligned}\frac{d\tilde{S}(x)}{dx} &= \frac{1}{4}gC_{g0}a_0^2\left[(iK)\left(\frac{2C_g - C/2}{CC_g}\right) + \frac{d}{dx}\left(\frac{2C_g - C/2}{CC_g}\right)\right]\\ &\times\exp\left(i\int_0^x K\,dx\right) = (iK)\tilde{S}\exp(i\Delta\Phi_{\tilde{S}_x}),\end{aligned} \tag{5.3}$$

where $\Delta\Phi_{\tilde{S}_x} \approx -K^{-1}[(2C_g - C/2)/CC_g]^{-1}\{(d/dx)[(2C_g - C/2)/CC_g]\}$ is the phase shift of radiation stress gradient due to its topography-induced amplitude change.

The energy transfer equation (5.1) may be rewritten as a function of these complex amplitudes,

$$W = -\frac{1}{2}\mathrm{Re}\left[\tilde{U}_{\mathrm{total}}\left(\frac{d\tilde{S}}{dx}\right)^{*}\right]$$
$$\equiv \frac{1}{2}K|\tilde{U}_{\mathrm{total}}||\tilde{S}|\sin(\Phi_{\tilde{U}_{\mathrm{total}}} - \Phi_{\tilde{S}} - \Delta\Phi_{\tilde{S}_x}), \tag{5.4}$$

where the superscript asterisk denotes the conjugate of the variable and $\Phi_{\tilde{U}_{\mathrm{total}}}$ and $\Phi_{\tilde{S}}$ are the phases of $\tilde{U}_{\mathrm{total}}$ and $\tilde{S}$. At constant water depth, (5.2) and (5.3) reduce to

$$\tilde{U}^{(0)}_{\mathrm{total}}(x) = \frac{1}{4}gC_{g0}a_0^2\left(\frac{C_g}{h}\eta_F^{(0)}\right)\exp\left(i\int_0^x K\,dx\right) \quad \text{and} \tag{5.5}$$

$$\frac{d\tilde{S}^{(0)}(x)}{dx} = \frac{1}{4}gC_{g0}a_0^2(iK)\left(\frac{2C_g - C/2}{CC_g}\right)\exp\left(i\int_0^x K\,dx\right)$$
$$= iK\tilde{S}^{(0)}(x). \tag{5.6}$$

In the constant water depth, the phase lead of the long wave relative to the short-wave group, $\Phi_{\tilde{U}_{\mathrm{total}}} - \Phi_{\tilde{S}}$ is zero and so is $\Delta\Phi_{\tilde{S}_x}$; therefore, according to (5.4), the energy transfer from the short-wave groups to the long waves becomes zero. In the variable water depth, the energy transfer is no longer zero, because the surface elevation and radiations stress components induced by variable water depth are in quadrature with their constant water depth counterparts. Accordingly, there are three different types of mechanisms that may contribute to the energy transfer at the leading order:

Mechanism 1: According to (3.7e), the forced long wave induced by depth variation $\eta_F^{(1)}(x)$ is linear in h_x and in quadrature with its constant-depth counterpart $\eta_F^{(0)}(x)$; therefore, it contributes to the energy transfer at the leading order. At variable water depth, the free long waves in the second square bracket of (5.2) are also generated, which propagate at a different speed from the short-wave group. It follows that the phase difference between the forward/backward free wave and the short-wave group, $\Phi_{\tilde{U}} - \Phi_{\tilde{S}}$, has an x-dependent component of $\int_0^x (K_h - K)\,dx / -\int_0^x (K_h + K)\,dx$ [cf. (5.2)]. This would cause the energy transfer to oscillate along the variable water depth.

Mechanism 2: The third square bracket of (5.2) is the U contributed by the topography-induced volume flux change. It is in quadrature with its constant-depth counterpart (5.5) and therefore contributes to the energy transfer to the long waves. This term has been included in Henderson et al.'s (2006) but not Battjes et al.'s (2004) studies of energy transfer between short-wave groups and shoaling long waves on a natural beach.

Mechanism 3: The second term on the right-hand side of (5.3) is the radiation stress gradient component due to topography-induced amplitude change of radiation stress, which is in quadrature with its counterpart for constant water depth (5.6) and therefore also contributes to the energy transfer to long waves. This term is assumed to be negligible in the shoaling zone before wave breaking (Battjes et al. 2004).

6. Example results

In this section, we evaluate the forced long waves $\tilde{\eta}_F^{(0)}$ and $[\tilde{\eta}_F^{(1)} + \tilde{\eta}_F^{(2)}]$, free long waves $\tilde{\eta}_+$ and $\tilde{\eta}_-$ induced by short-wave groups over plane and sinusoidal ramps, and Gaussian and sinusoidal canyons and ridges connecting with constant depths, with special attention to the effect of discontinuity in depth derivatives h_x and h_{xx} at the junctions. Each of these pairs has similar $h(x)$ but different h_x and h_{xx} at the junctions.

a. Plane ramps

We first consider a sinusoidally modulated wave train over a downward sloping plane ramp connecting two constant water depths,

$$h = \tilde{h}(1 + x/L)/2, \quad (0 \le x \le L)$$
$$h = \tilde{h}/2, \quad (x < 0)$$
$$h = \tilde{h}, \quad (x > L), \tag{6.1a}$$

and an upward sloping plane ramp connecting two constant water depths,

$$h = 3\tilde{h}/2 - \tilde{h}(1 + x/L)/2, \quad (0 \le x \le L)$$
$$h = \tilde{h}, \quad (x < 0)$$
$$h = \tilde{h}/2, \quad (x > L), \tag{6.1b}$$

where L is the width of the ramp. Figures 2a,b illustrate water depth variation, whereas Figs. 2c,d demonstrate the amplitude variations of $\tilde{\eta}_F^{(0)}$, $[\tilde{\eta}_F^{(1)} + \tilde{\eta}_F^{(2)}] + \tilde{\eta}_+ + \tilde{\eta}_-$, $[\tilde{\eta}_F^{(1)} + \tilde{\eta}_F^{(2)}]$, $\tilde{\eta}_+$, and $\tilde{\eta}_-$ over $0 < x < L$ for a ramp width of $L = 10/\varepsilon k_\infty$. We note that the transmitted free wave is larger than the reflected one for both downward and upward sloping ramps.

For the downward sloping ramp, the forced wave (dashed line) attains maximum magnitude at the incident edge where water depth is at minimum. A forward free

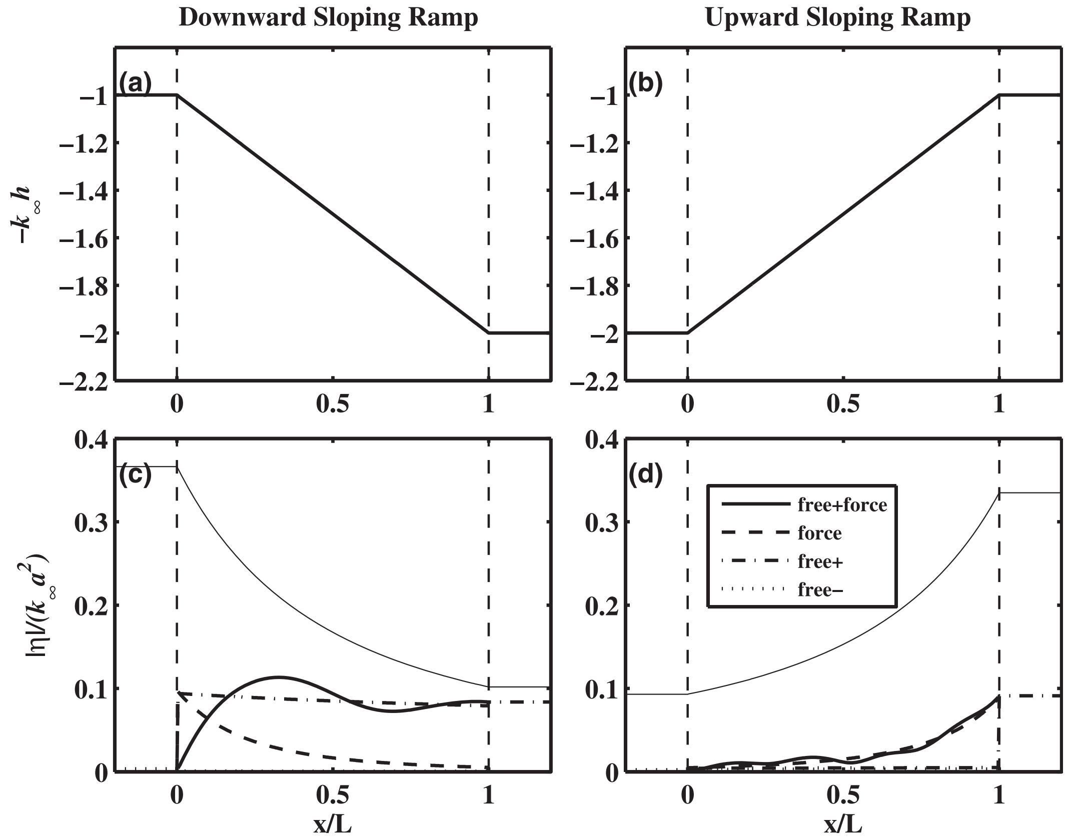

FIG. 2. Amplitude of group bound long waves induced by variable depth $[\tilde{\eta}_F^{(1)} + \tilde{\eta}_F^{(2)}]$ (thick dashed lines) and forward (dashed–dotted lines) and backward (dotted lines) propagating free long waves $\tilde{\eta}_+$ and $\tilde{\eta}_-$, and the sum of these three waves (thick solid lines) over a (left) downward and (right) upward sloping plane ramp. The thin solid line denotes the constant-depth forced wave $\tilde{\eta}_F^{(0)}$ locked to the wave group, and the two vertical dashed lines indicate the topography edges. The width of the ramp is $L = 10/\varepsilon k_\infty$.

wave (dashed–dotted line) of similar amplitude is generated here. Then the magnitude of the forced wave decays rapidly along the ramp, whereas that of free wave decreases only slightly (Fig. 2c). The backward free wave is negligible across the ramp in comparison with these two waves.

For the upward sloping ramp, the forced wave starts with near-zero amplitude at the incident edge where the water depth is at maximum, and then it increases in magnitude rapidly along the ramp and generates a forward free wave of similar amplitude at the transmission edge. Both the backward and forward free waves are negligible across the ramp in comparison with the forced wave (Fig. 2d).

The topography-induced long wave {i.e., forced + free long wave $[\tilde{\eta}_F^{(1)} + \tilde{\eta}_F^{(2)}] + \tilde{\eta}_+ + \tilde{\eta}_-$} is equivalent to ξ_F of Mei and Benmoussa (1984) and Liu (1989). As shown by the solid line in Figs. 2c,d, for both upward and downward sloping ramps, the topography-induced forced wave $[\tilde{\eta}_F^{(1)} + \tilde{\eta}_F^{(2)}]$ (solid lines) has the same trend as the constant-depth forced wave $\tilde{\eta}_F^{(0)}$ (thin solid line) over the topography between two vertical dashed lines. Here, $[\tilde{\eta}_F^{(1)} + \tilde{\eta}_F^{(2)}] + \tilde{\eta}_+ + \tilde{\eta}_-$ is near zero at the incident edge ($x = 0$) and increases over the ramp toward a much larger value at the transmission edge ($x = L$). According to (4.1e) and (4.1f), this leads to the results shown in Figs. 2c,d that, for both types of ramp, the transmitted wave is larger than the reflected wave. We also note that $[\tilde{\eta}_F^{(1)} + \tilde{\eta}_F^{(2)}] + \tilde{\eta}_+ + \tilde{\eta}_-$ displays a convex/concave trend over a downward/upward sloping ramp. This is mainly because $[\tilde{\eta}_F^{(1)} + \tilde{\eta}_F^{(2)}]$ is inversely proportional to $(1 - gh/C_g^2)$ according to (3.7), so that they decrease with the relative water depth $k_\infty h$ while $\tilde{\eta}_+$ and $\tilde{\eta}_-$ are proportional to $h^{-1/4}$, so that its amplitude only change slightly over the topography.

To examine the effect of topography width on long waves, we increase L to $L = 30/\varepsilon k_\infty$ while keeping the depth difference $\Delta h = h_1 - h_0$ the same. As shown in Fig. 3, the magnitudes of all long waves are reduced for milder bottom slope. Although the trends of amplitude

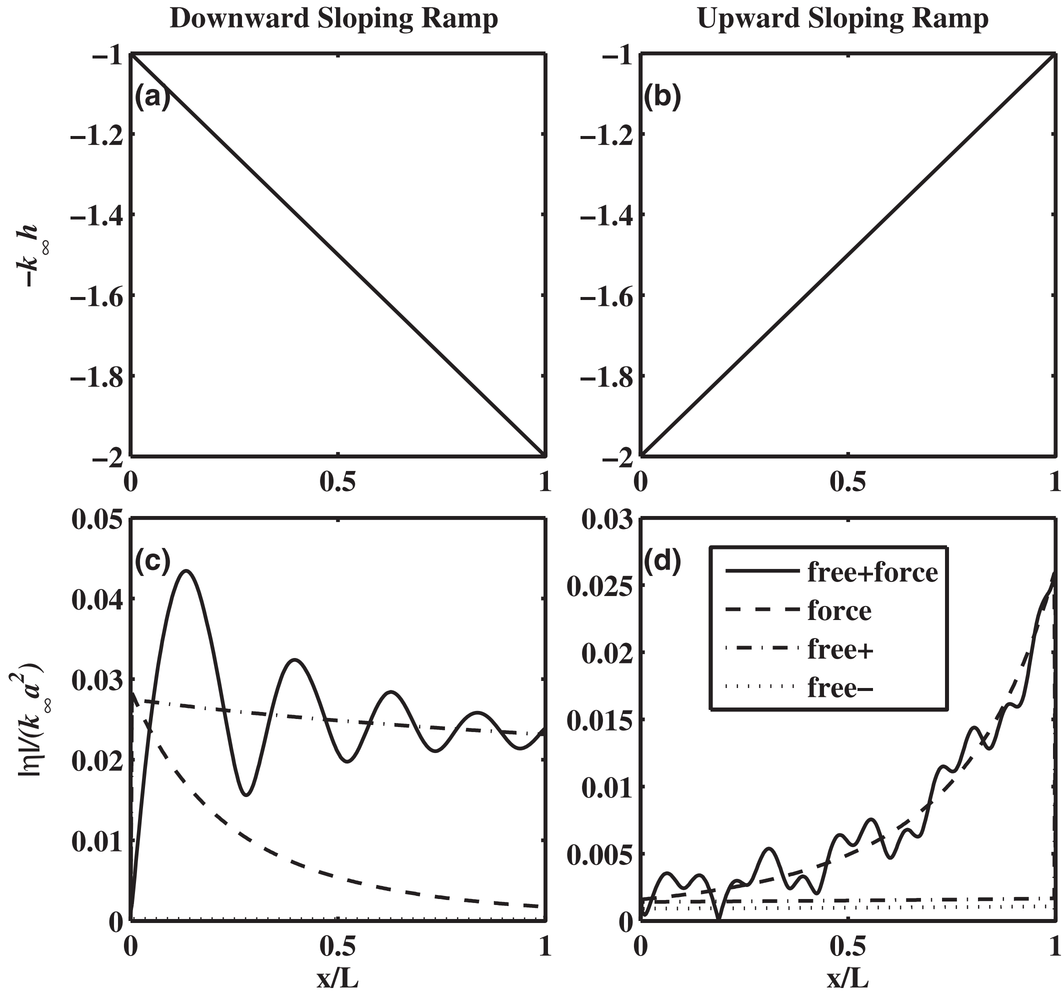

FIG. 3. As in Fig. 2, but for a ramp width of $L = 30/\varepsilon k_\infty$.

variation of these waves resemble those in Fig. 2, an additional oscillatory variation starts to appear in the $[\tilde{\eta}_F^{(1)} + \tilde{\eta}_F^{(2)}] + \tilde{\eta}_+ + \tilde{\eta}_-$ (solid line) along the downward sloping ramp. This oscillatory behavior is caused by the interference between the forward propagating free wave and the forced waves over the topography discussed in the last paragraph of section 4. The oscillation is larger for the downward sloping ramp over which these two waves become comparable in magnitude; therefore, the interference is enhanced (Fig. 3c).

To investigate the effect of topography width and water depth on the amplitude of transmitted and reflected free waves, we calculate T and R for $k_\infty \tilde{h} = 2, 3,$ and 4 and $10 \le \varepsilon k_\infty L \le 30$, and the results are given by Fig. 4. As shown by Fig. 4, for the upward and downward sloping plane ramp, the transmitted and reflected waves show similar magnitude and variations with relative water depth and width of topography. The reflected wave is much smaller than the transmitted wave. Small oscillatory variations in the amplitude start to develop at relatively deeper water because of the interference between the free waves and the forced waves (Figs. 4e,f). As discussed in the last paragraph of section 4, the amplitudes of reflected and transmitted waves are proportional to the bottom slope h_x and inversely proportional to $(1 - gh/C_g^2)$ according to (3.7); therefore, they decrease with the relative water depth $k_\infty h$ and relative width of topography $k_\infty L$, as shown in Fig. 4.

The energy transfer from the short-wave groups to long waves according to (5.4) is indicated by the solid lines in Fig. 5 (middle and bottom) and oscillates between positive and negative values along the downward sloping ramp, which corresponds to increase and decrease in the amplitude of long wave given by Fig. 5 (top). The energy transfer increases almost monotonically along the upward sloping ramp, resembling the shoaling behavior of long-wave amplitude in Fig. 5 (top). Because of the very mild bottom slope in this case, the topography-induced

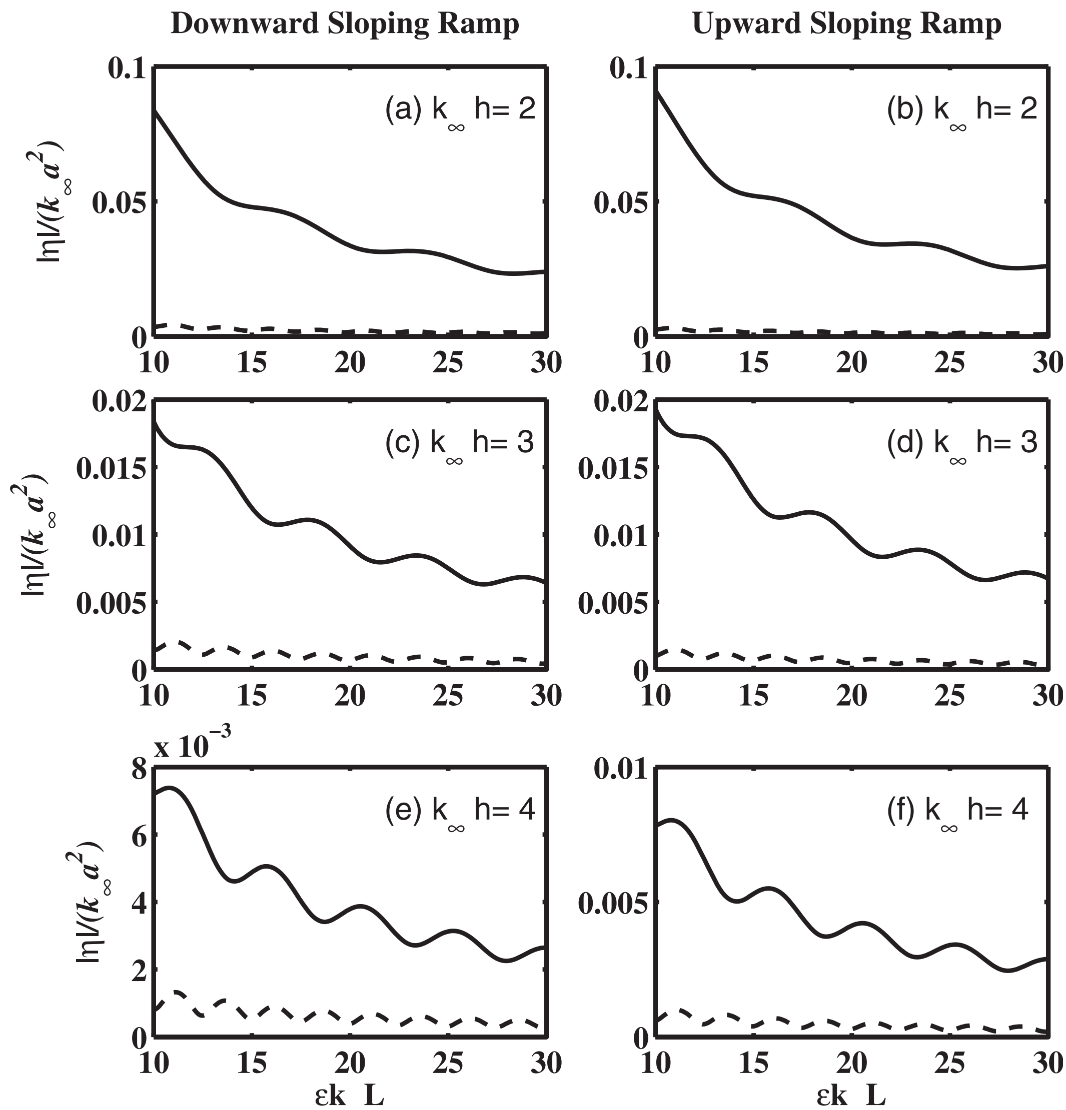

FIG. 4. Amplitudes of forward (solid lines) and backward (dashed lines) scattered free long waves at the transmission/incident side of the (left) downward and (right) upward sloping plane ramps (6.1) as a function of relative ramp width $k_\infty L$ for water depths of $k_\infty h =$ (top) 2 ($h = \tilde{h}$, the maximum water depth), (middle) 3, and (bottom) 4.

amplitude change of radiation stress has a negligible contribution to the energy transfer (Fig. 5, middle), whereas the topography-induced volume flux has a significant contribution to the energy transfer (Fig. 5, bottom) only at the shallow part of the topography. These contributions, however, are expected to increase with bottom slope and decreasing water depth where the normalized bed slope h_x/Kh is larger and become significant near a bar at a beach (Battjes et al. 2004; Henderson et al. 2006).

b. Sinusoidal ramps

We next consider a wave train over a downward sloping sinusoidal ramp,

$$h = \tilde{h}\{1 + \sin^2[\pi x/(2L)]\}/2, \quad (0 \le x \le L)$$
$$h = \tilde{h}/2, \quad (x < 0)$$
$$h = \tilde{h}, \quad (x > L), \tag{6.2a}$$

and an upward sloping sinusoidal ramp,

$$h = 3\tilde{h}/2 - \tilde{h}\{1 + \sin^2[\pi x/(2L)]\}/2, \quad (0 \le x \le L)$$
$$h = \tilde{h}, \quad (x < 0)$$
$$h = \tilde{h}/2, \quad (x > L), \tag{6.2b}$$

where L is the width of the ramp. Topography (6.2) is similar to (6.1), except at the junctions the former has

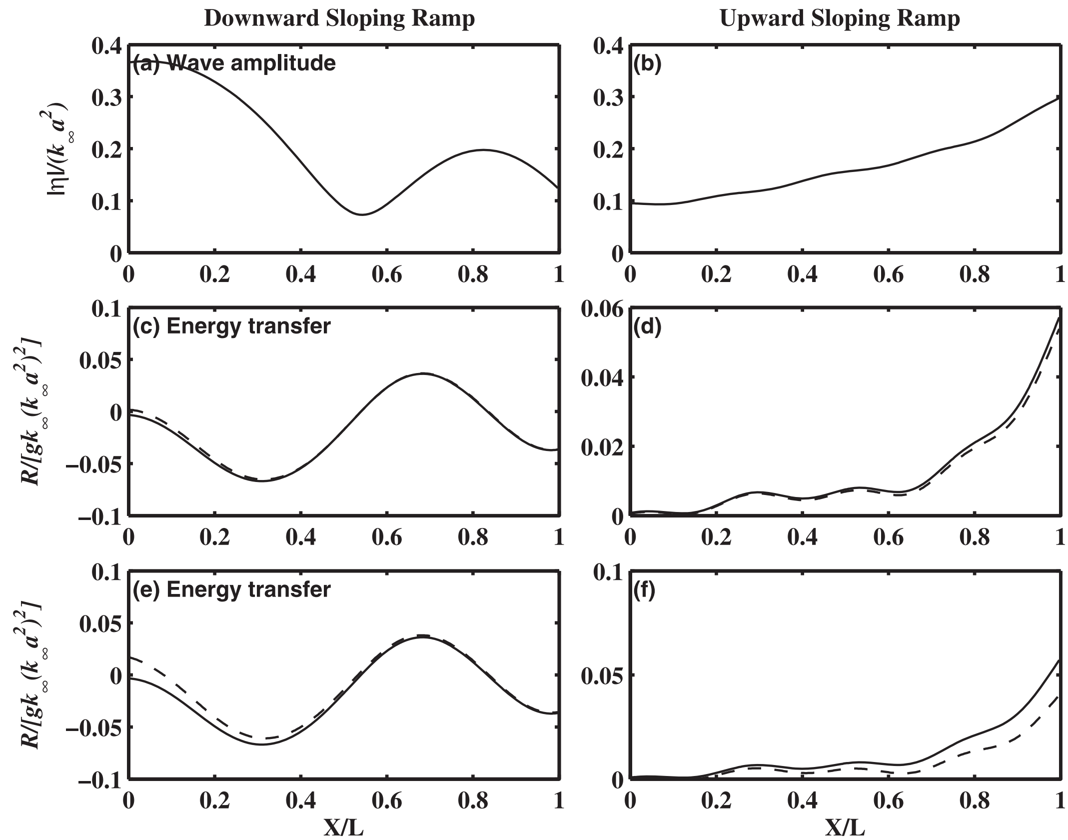

FIG. 5. Long-wave amplitude and energy transfer from short-wave group to long wave for a (left) downward and (right) upward sloping ramp: (a),(b) amplitude of total long wave (bound + force + free); (c),(d) energy transfer from short-wave group to long wave, with (solid lines) and without (dashed lines) amplitude gradient of radiation stress [cf. Eq. (5.3)]; (e),(f) energy transfer, with (solid lines) and without (dashed lines) amplitude change of U [cf. Eq. (5.2)]. The width of the ramp is $L = 10/\varepsilon k_\infty$. Water depth is $k_\infty h = 2$ ($h = \tilde{h}$, the maximum water depth).

continuous h_x and h and discontinuous h_{xx}, whereas the latter has continuous h and h_{xx} and discontinuous h_x.

The amplitudes for transmitted and reflected waves for $k_\infty \tilde{h} = 2, 3$, and 4 and for $10 \le \varepsilon k_\infty L \le 30$ are given by Fig. 6 for the downward and upward sloping sinusoidal ramps. The radiating free waves are smaller than their counterparts for plane ramps shown in Fig. 4, because h_x is zero at the topography junctions so that T and R are now on the order of $O(h_{xx})$ [cf. (A3) and (A4)]. In addition, the oscillatory variation of radiating waves is reduced because the forced wave is much stronger than the free wave over the topography; therefore, the interference between them is weakened.

c. Gaussian canyon and ridge

We now consider a Gaussian canyon,

$$h = \tilde{h}\exp\left[-\alpha\left(\frac{x}{L}-\frac{1}{2}\right)^2\right], \quad (0 \le x \le L)$$
$$h = \tilde{h}/2, \quad (x < 0 \quad \text{and} \quad x > L), \tag{6.3a}$$

and a Gaussian ridge,

$$h = \tilde{h}\left\{\frac{3}{2} - \exp\left[-\alpha\left(\frac{x}{L}-\frac{1}{2}\right)^2\right]\right\}, \quad (0 \le x \le L)$$
$$h = \tilde{h}, \quad (x < 0 \quad \text{and} \quad x > L), \tag{6.3b}$$

where $\alpha = 4(\log 2)$ and L is the width of the canyon and ridge. As shown by Fig. 7, the amplitude variations of free and forced waves along the first half of the canyon/ridge is similar to those along the downward/upward sloping plane ramp (cf. Fig. 2). The amplitudes of free and forced waves are symmetric about the center of the topography, but the amplitude of the sum of these two, $[\tilde{\eta}_F^{(1)} + \tilde{\eta}_F^{(2)}] + \tilde{\eta}_+ + \tilde{\eta}_-$, is not. As in the cases of linear ramp, the transmitted wave is stronger than the reflected wave for both canyon and ridge. In addition, the topography-induced forced wave $[\tilde{\eta}_F^{(1)} + \tilde{\eta}_F^{(2)}]$ (solid lines) has the same trend as the constant-depth forced wave solution $\tilde{\eta}_F^{(0)}$ (thin solid line) over the topography between the two vertical dashed lines.

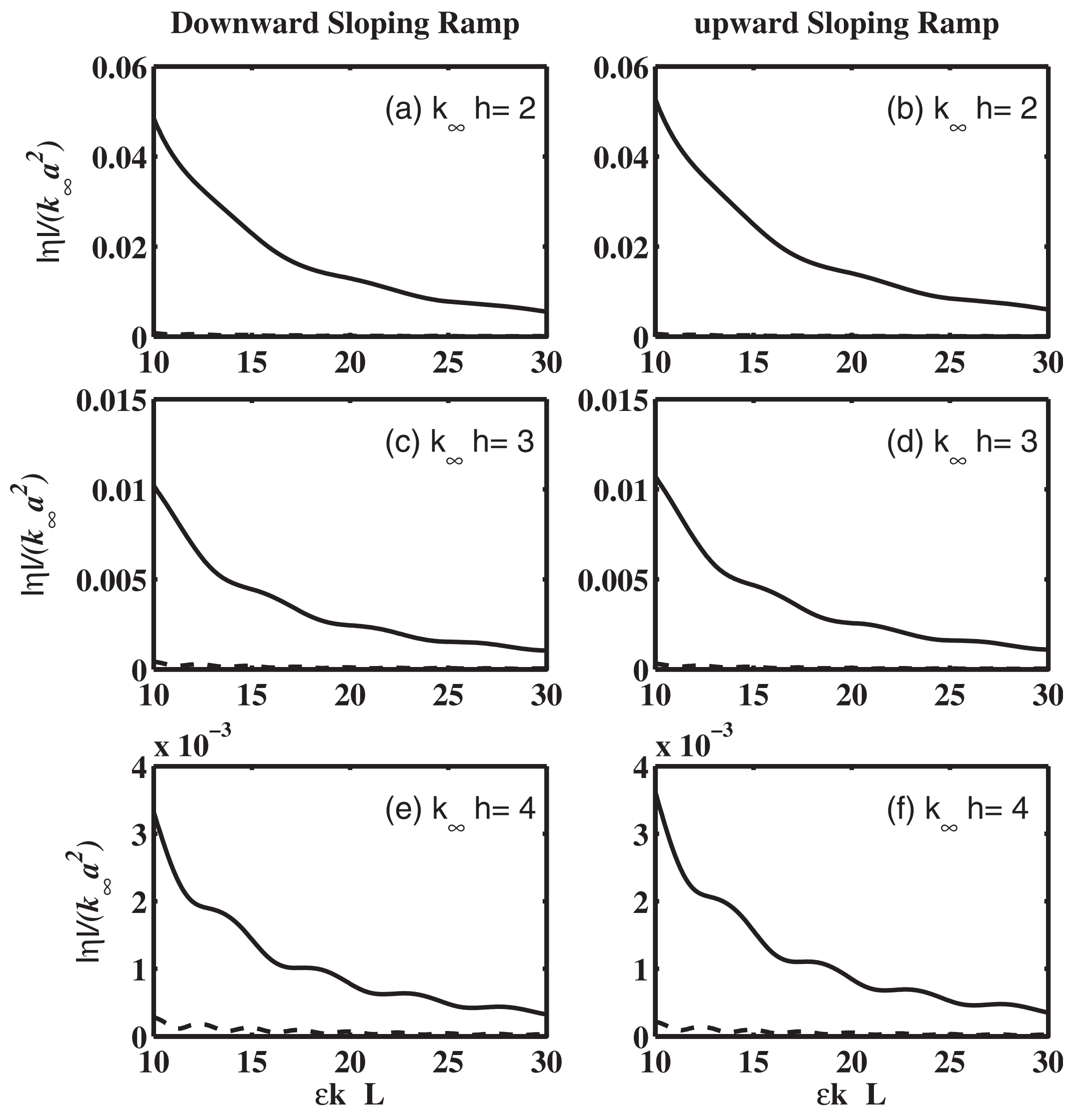

FIG. 6. Amplitude of forward (solid lines) and backward (dashed lines) scattered free long waves at the transmission/incident side of the (left) downward and (right) upward sloping sinusoidal ramps (6.2) as a function of relative ramp width $k_\infty L$ for water depths of $k_\infty h$ = (top) 2 ($h = \tilde{h}$, the maximum water depth), (middle) 3, and (bottom) 4.

For a canyon, the forced wave $[\tilde{\eta}_F^{(1)} + \tilde{\eta}_F^{(2)}]$ (dashed line) attains maximum at the incident edge where the water depth is minimum. A forward propagating free wave (dashed–dotted line) of similar amplitude is generated here. Then the magnitude of the forced wave decays rapidly to a minimum at the center of the canyon and increases to a maximum at the transmission edge. The amplitude variation of the forward propagating free wave has the same trend but at much smaller rate (Fig. 7). The backward free wave (dotted line) is negligible across the ramp in comparison with these two waves.

For a ridge, the forced wave starts with near-zero amplitude at the incident edge where water depth is at maximum and then increases in magnitude rapidly to a maximum at the center of the ridge and decreases to a minimum and generates a forward propagating free wave of similar amplitude at the transmission edge. Both the backward and forward free waves are negligible in the middle of the ridge in comparison with the forced waves (Fig. 7).

The amplitude of transmitted/reflected free waves (solid/dashed lines) for a relative water depth $k_\infty \tilde{h} = 2, 3,$ and 4 and relative topography width $10 \leq \varepsilon k_\infty L \leq 30$ are given in Fig. 8. As shown by Fig. 8, the amplitudes of transmitted and reflected free waves oscillate between local maximums and zeros. Similar to the results for ramps shown in Fig. 4, the amplitudes of transmitted and reflected waves decrease with relative topography width

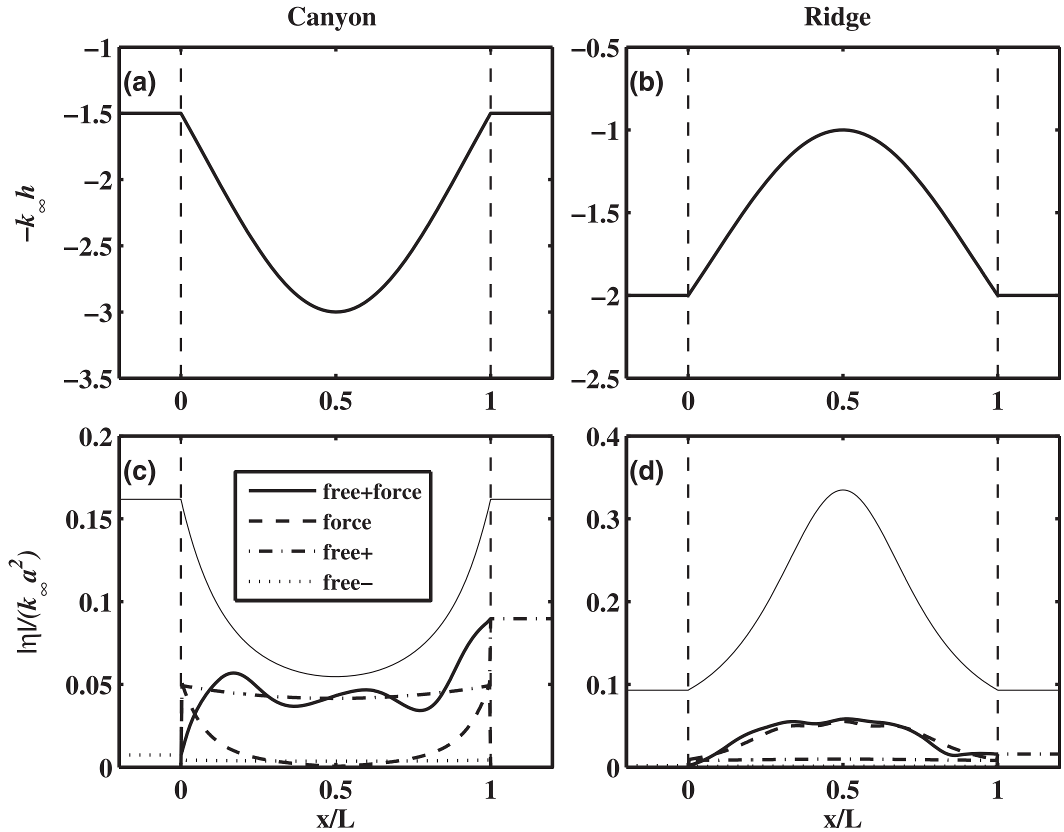

FIG. 7. Amplitude of group bound long waves induced by variable depth $[\tilde{\eta}_F^{(1)} + \tilde{\eta}_F^{(2)}]$ (thick dashed lines) and forward (dashed–dotted lines) and backward (dotted lines) propagating free long waves $\tilde{\eta}_+$ and $\tilde{\eta}_-$ and the sum of these three waves (thick solid lines) over a Gaussian (left) canyon and (right) ridge. The thin solid line denotes the constant-depth forced wave $\tilde{\eta}_F^{(0)}$ locked to the wave group, and the two vertical dashed lines indicate the topography edges. The width of the ramp is $L = 15/\varepsilon k_\infty$. The water depth is (a),(c) $k_\infty \tilde{h} = 2$ and (b),(d) $k_\infty \tilde{h} = 4$ ($\tilde{h}$ is the maximum water depth).

$k_\infty L$ and decrease with relative water depth $k_\infty \tilde{h}$. However, the oscillatory variation of amplitude with the relative topography width is stronger because of enhanced interference of free and forced waves for canyon and ridge when these two waves become comparable in magnitude. The local maximums decrease with relative topography width and water depth. The reflected wave is much smaller than the transmitted one.

Long waves are largely dependent on local water depth. For a canyon (Fig. 8c) and a ridge (Fig. 8b) that have the same depths at $x = \pm\infty$, the transmitted and reflected free waves have the same order of magnitude. As discussed at the last paragraph of section 4, the magnitude of transmitted and reflected free wave is determined by that of the free + topography-induced force wave, $[\tilde{\eta}_F^{(1)} + \tilde{\eta}_F^{(2)}] + \tilde{\eta}_+ + \tilde{\eta}_-$, at the edge of the topography. As shown in Figs. 8b,c, the canyon would generate slighter larger free waves because $[\tilde{\eta}_F^{(1)} + \tilde{\eta}_F^{(2)}] + \tilde{\eta}_+ + \tilde{\eta}_-$ is more enhanced at the edge of canyon than ridge (Fig. 7).

The energy transfer from the short-wave groups to long waves according to (5.4) is indicated by the solid lines in Fig. 9 (middle and bottom) and oscillates between positive and negative values along canyon and ridge corresponding to increase and decrease in the amplitude of the long wave in Fig. 6 (top). The topography-induced amplitude change of radiation stress (dashed lines in Fig. 9, middle) and volume flux (dashed lines in Fig. 9, bottom) have a significant contribution to the energy transfer, especially at the shallow part of the topography and where the bottom slope is at its maximum.

d. Sinusoidal canyon and ridge

Finally, we consider a sinusoidal canyon,

$$h = \tilde{h}[1 + \sin^2(\pi x/L)]/2 \quad (0 \le x \le L)$$
$$h = \tilde{h}/2, \quad (x < 0 \quad \text{and} \quad x > L), \qquad (6.4a)$$

and a sinusoidal ridge,

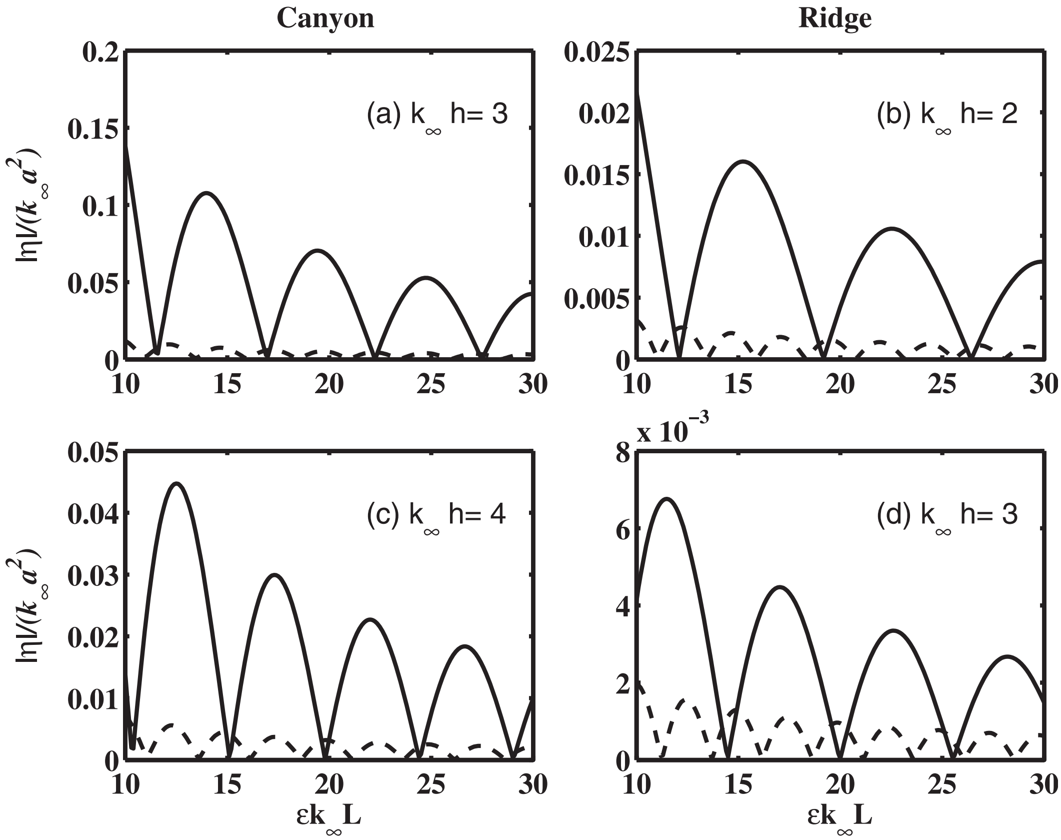

FIG. 8. Amplitude of forward (solid lines) and backward (dashed lines) scattered free long waves at the transmission/incident side of Gaussian (left) canyon and (right) ridge as a function of relative topography width $k_\infty L$ for a water depth of $k_\infty h$ = 2–4 ($h = \tilde{h}$, the maximum water depth).

$$h = 3\tilde{h}/2 - \tilde{h}\{1 + \sin^2[\pi x/(L)]\}/2, \quad (0 \le x \le L)$$
$$h = \tilde{h}, \quad (x < 0 \quad \text{and} \quad x > L), \tag{6.4b}$$

where L is the width of the canyon and ridge. The calculated results for T and R for $k_\infty \tilde{h} = 2$, 3, and 4; for $5 \le \varepsilon k_\infty L \le 30$; and for sinusoidal canyon and ridge (not shown here) indicate that the radiating free waves in both directions are smaller than their counterparts for the Gaussian canyon and ridge because h_x approaches zero on both sides of the topography junctions. Similar to those of sinusoidal ramps (Fig. 6), the oscillatory variation of radiating free waves with relative topography width is reduced by the weakened interference of forced and free waves because the former is much larger than the latter.

7. Conclusions and discussion

As short-wave groups encounter a localized topography, free long waves radiate away from the region at a shallow-water wave speed of $\sqrt{gh}$. The transmitted free wave is stronger than the reflected free wave for all types of topography because of the mild bottom slope used in this study. The amplitude of these scattered free waves increases with decreasing water depth and wave frequency. For canyon/ridge type topography, the amplitudes of these waves decrease with topography width in an oscillatory fashion, whereas, for ramp type topography, their amplitudes decrease with the topography width almost monotonically. We also note that the amplitude of the sum of free and topography-induced forced waves, $[\tilde{\eta}_F^{(1)} + \tilde{\eta}_F^{(2)}] + \tilde{\eta}_+ + \tilde{\eta}_-$, displays an oscillatory variation along a topography whose width is sufficiently larger than the group wavelength. These oscillatory behaviors are due to the interference of free and forced waves over the topography. These behaviors were not resolved by previous numerical models, which only calculate the total amplitude of the sum of free and topography-induced forced waves, $[\tilde{\eta}_F^{(1)} + \tilde{\eta}_F^{(2)}] + \tilde{\eta}_+ + \tilde{\eta}_-$.

Although the variable water depth–induced forced and free long waves represent a second-order correction to the total magnitude of long waves over a mild slope,

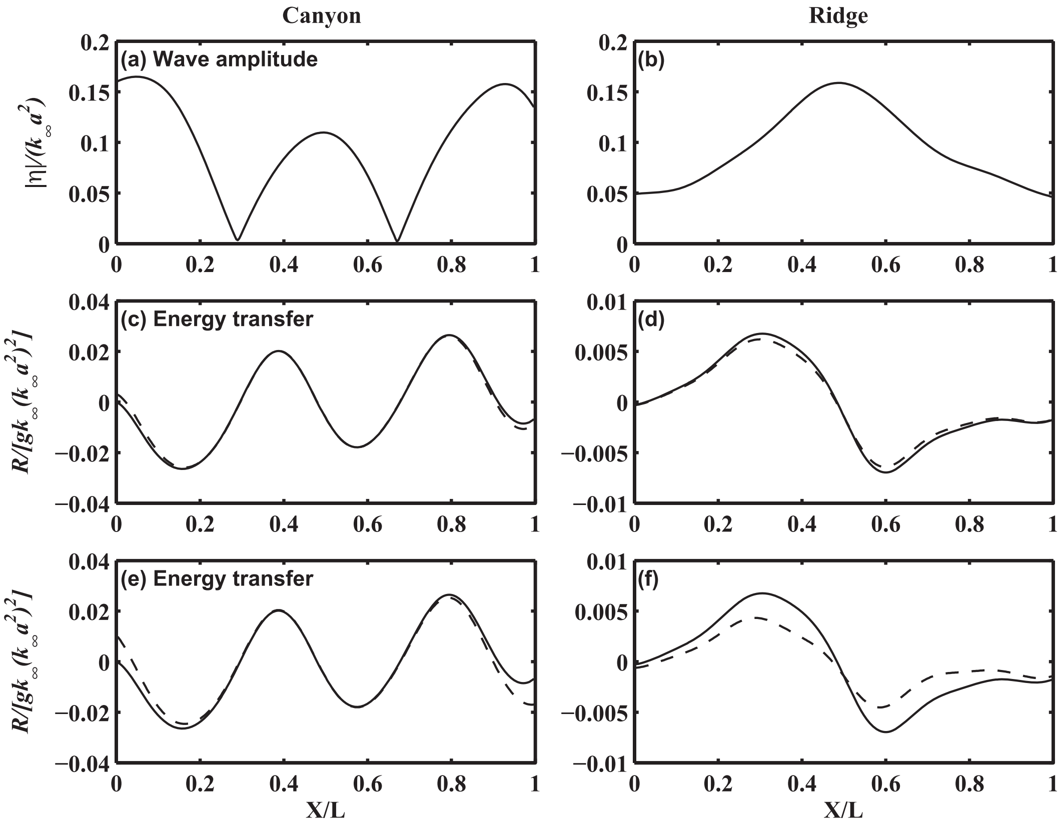

FIG. 9. Long-wave amplitude and energy transfer from short-wave group to long waves for a (left) canyon and (right) ridge. Lines and symbols are as in Fig. 5. The width of the ramp is $L = 12/\varepsilon k_\infty$. Water depth is $k_\infty h = 3$ ($h = \tilde{h}$, the maximum water depth).

they contribute to the phase shift and therefore the energy transfer between the short-wave group and long wave at the leading order because they are out of phase with the wave group. In addition, the gradient of short-wave radiation stress is modified by the presence of topography, so is the current associated with long waves as required by mass conservation. These modifications are in quadrature with their constant water depth counterparts and therefore result in leading-order contributions to the energy transfer. These three mechanisms for energy transfer between wave group and long waves for a finite topography have not been explored in the literature.

Our analytical results indicate that the inclusion of the bottom slope terms in the long-wave solutions is necessary to fully describe topographic scattering of long waves. The scattered waves are weakened in the case of a smooth topography junction where discontinuity of h_x becomes negligible. In the cases of sinusoidal ramp, canyon, and ridge (cf. Fig. 6), both h and h_x are continuous at the junctions, but h_{xx} and the slope of $[\tilde{\eta}_F^{(1)} + \tilde{\eta}_F^{(2)}] + \tilde{\eta}_+ + \tilde{\eta}_-$ are discontinuous. In these cases, the presence of scattered free waves must be due to the discontinuities in h_{xx}.

Mei and Benmoussa (1984) and Liu (1989) solved a governing equation equivalent to (2.6) numerically by a finite-element method. They assume that the length scale of the topography is at the same order as the wavelength of the wave group; that is, $h_x/Kh = O(1)$, $h_{xx}/Kh = O(1)$. In contrast, our asymptotic expansion solutions to the problem are valid only if the former is one order of magnitude larger than the latter; that is, $h_x/Kh = O(\mu)$, $h_{xx}/Kh = O(\mu^2)$. Therefore, we are unable to conduct quantitative comparisons between the present analytical solutions and the numerical results by Mei and Benmoussa (1984) and Liu (1989).

Despite the present solution being only valid for a mild slope, the tractability of the analytical solution allows us to reveal some new physics described above regarding wave-group-induced forced and free waves over varying depth by paying special attention to the topography-induced phase change of these long waves and interference between forced and free long waves. The effect of these processes should be enhanced at a steeper slope and shallower water where the normalized bed slope h_x/Kh is large.

Acknowledgments. The author is indebted to Professor John. W. Miles for guidance and advice. The author would like to thank Professor D. H. Peregrine for valuable comments and suggestions about this manuscript. This work was supported in part by the Flood Risk from Extreme Events (FREE) Programme of the UK Natural Environment Research Council (NERC) (NE/E0002129/1) and by the Office of Naval Research Grant N00014-92-J-1171.

APPENDIX

Second-Order Free Wave Amplitude Coefficients

Substituting (3.7)–(3.10) and (3.3b) into (4.1), at the second order, we have

$$\begin{aligned} C_+ &= -\frac{1}{2}\left\{\left(1+\frac{\sqrt{gh_0}}{C_{g0}}\right)[\eta_F^{(1)}(0^+)+\eta_F^{(2)}(0^+)]+\sqrt{gh_0}(i\Omega)^{-1}[\eta_{Ex}^{(0)}(0^+)+\eta_x^{(1)}(0^+)]\right\} \\ &\quad\times\left[\eta_+^{(0)}(0^+)+\eta_+^{(1)}(0^+)+\frac{1}{2}\sqrt{gh_o}(i\Omega)^{-1}\eta_{+x}^{(0)}(0^+)\right]^{-1}+O(h_x^3,h_xh_{xx},h_{xxx}) \\ &\equiv C_+(k_\infty,h,L,h_x,h_{xx})+O(h_x^3,h_xh_{xx},h_{xxx}), \end{aligned} \tag{A1}$$

$$\begin{aligned} C_- &= -\frac{1}{2}\left\{\left(1-\frac{\sqrt{gh_1}}{C_{g1}}\right)[\eta_F^{(1)}(L^-)+\eta_F^{(2)}(L^-)]-\sqrt{gh_1}(i\Omega)^{-1}[\eta_{Ex}^{(0)}(L^-)+\eta_x^{(1)}(L^-)]\right\} \\ &\quad\times\left[\eta_-^{(0)}(L^-)+\eta_-^{(1)}(L^-)-\frac{1}{2}\sqrt{gh_1}(i\Omega)^{-1}\eta_{-x}^{(0)}(L^-)\right]^{-1}\exp\left[i\int_{0^+}^{L^-}(K+K_h)\,dx\right]+O(h_x^3,h_xh_{xx},h_{xxx}) \\ &\equiv C_-(k_\infty,h,L,h_x,h_{xx})+O(h_x^3,h_xh_{xx},h_{xxx}), \end{aligned} \tag{A2}$$

$$\begin{aligned} T &= [\eta_+^{(0)}(L^+)]^{-1}\left\{[\eta_F^{(1)}(L^-)+\eta_F^{(2)}(L^-)]\exp\left[i\int_{0^+}^{L^-}(K-K_h)\,dx\right]\right. \\ &\quad\left.+C_+[\eta_+^{(0)}(L^-)+\eta_+^{(1)}(L^-)]+C_-[\eta_-^{(0)}(L^-)+\eta_-^{(1)}(L^-)]\exp\left(-2i\int_{0^+}^{L^-}K_h\,dx\right)\right\}+O(h_x^3,h_xh_{xx},h_{xxx}) \\ &\equiv T(k_\infty,h,L,h_x,h_{xx})+O(h_x^3,h_xh_{xx},h_{xxx}), \end{aligned} \tag{A3}$$

and

$$\begin{aligned} R &= [\eta_-^{(0)}(0^+)]^{-1}\{\eta_F^{(1)}(0^+)+\eta_F^{(2)}(0^+)+C_+[\eta_+^{(0)}(0^+)+\eta_+^{(1)}(0^+)]+C_-[\eta_-^{(0)}(0^+)+\eta_-^{(1)}(0^+)]\}+O(h_x^3,h_xh_{xx},h_{xxx}) \\ &\equiv R(k_\infty,h,L,h_x,h_{xx})+O(h_x^3,h_xh_{xx},h_{xxx}), \end{aligned} \tag{A4}$$

where h_0, C_{g0} and h_1, C_{g1} are the values taken by h and C_g in the regions $x < 0$ and $x > L$, respectively, and $K = \Omega/C_g$ and $K_h = \Omega/\sqrt{gh}$ are the wavenumbers for forced and free waves.

REFERENCES

Battjes, J. A., H. J. Bakkenes, T. T. Janssen, and A. R. van Dongeren, 2004: Shoaling of subharmonic gravity waves. *J. Geophys. Res.,* **109,** C02009, doi:10.1029/2003JC001863.

Chu, V. H., and C. C. Mei, 1970: On slowly varying Stokes waves. *J. Fluid Mech.,* **41,** 873–887.

Davey, A., and K. Stewartson, 1974: On three-dimensional packets of surface waves. *Proc. Roy. Soc. London,* **388A,** 101–110.

Djordjevic, V. D., and L. G. Redekopp, 1977: On two-dimensional packets of capillary-gravity waves. *J. Fluid Mech.,* **79,** 703–714.

Elgar, S., and R. T. Guza, 1985: Observations of bispectra of shoaling surface gravity waves. *J. Fluid Mech.,* **161,** 425–448.

Hasimoto, H., and H. Ono, 1972: Nonlinear modulation of gravity waves. *J. Phys. Soc. Japan,* **33,** 805.

Hasselmann, K., W. Munk, and G. MacDonald, 1963: Bispectra of ocean waves. *Proceedings of the Symposium on Time Series Analysis,* M. Rosenblatt, Ed., SIAM Series in Applied Math, Wiley, 125–139.

Henderson, S. M., R. T. Guza, S. Elgar, T. H. C. Herbers, and A. J. Bowen, 2006: Nonlinear generation and loss of infragravity wave energy. *J. Geophys. Res.,* **111,** C12007, doi:10.1029/2006JC003539.

Herbers, T. H. C., S. Elgar, and R. T. Guza, 1995: Generation and propagation of infragravity waves. *J. Geophys. Res.,* **100,** 24 863–24 872.

Janssen, T. T., J. A. Battjes, and A. R. van Dongeren, 2003: Long waves induced by short-wave groups over a sloping bottom. *J. Geophys. Res.,* **108,** 3252, doi:10.1029/2002JC001515.

Kirby, J., and R. Dalrymple, 1983: Propagation of obliquely incident water waves over a trench. *J. Fluid Mech.,* **133,** 47–63.

Liu, P. L.-F., 1989: A note on long waves induced by short-wave groups over a shelf. *J. Fluid Mech.,* **205,** 163–170.

Longuet-Higgins, M. S., and R. W. Stewart, 1960: Changes in the form of short gravity waves on long waves and tidal currents. *J. Fluid Mech.,* **8,** 565–583.

——, and ——, 1961: The changes in amplitude of short gravity waves on steady non-uniform currents. *J. Fluid Mech.,* **10,** 529–549.

——, and ——, 1962: Radiation stress and mass transport in gravity waves, with application to 'surf beats.' *J. Fluid Mech.,* **13,** 481–504.

——, and ——, 1964: Radiation stresses in water waves: A physical discussion, with applications. *Deep-Sea Res.,* **11,** 529–562.

Mei, C. C., and C. Benmoussa, 1984: Long waves induced by short-wave groups over an uneven bottom. *J. Fluid Mech.,* **139,** 219–235.

Miles, J., and Q. Zou, 1992: Gravity wave reflection at a discontinuity in bottom slope. *J. Phys. Oceanogr.,* **23,** 1870–1871.

Munk, W., 1949: Surf beats. *Eos, Trans. Amer. Geophys. Union,* **30,** 849–854.

Okihiro, M., R. T. Guza, and R. J. Seymour, 1992: Bound infragravity waves. *J. Geophys. Res.,* **97,** 11 453–11 469.

Ono, H., 1991: Deformation of nonlinear gravity waves due to a depth variation. *J. Phys. Soc. Japan,* **60,** 4127–4132.

Phillips, O., 1977: *The Dynamics of the Upper Ocean*. 2nd ed. Cambridge University Press, 336 pp.

Thomson, J., S. Elgar, B. Raubenheimer, T. H. C. Herbers, and R. T. Guza, 2006: Tidal modulation of infragravity waves via nonlinear energy losses in the surfzone. *Geophys. Res. Lett.,* **33,** L05601, doi:10.1029/2005GL025514.

Tucker, M. J., 1950: Surf beats: Sea waves of 1 to 5 min. period. *Proc. Roy. Soc. London,* **202A,** 565–573.

Van Dongeren, A. R., A. J. H. M. Reniers, J. A. Battjes, and I. A. Svendsen, 2003: Numerical modeling of infragravity wave response during DELILAH. *J. Geophys. Res.,* **108,** 3288, doi:10.1029/2002JC001332.

Whitham, G. B., 1967: Non-linear dispersion of water waves. *J. Fluid Mech.,* **27,** 399–412.

——, 1974: *Linear and Nonlinear Waves*. Wiley, 636 pp.

Zou, Q.-P., 1995: A viscoelastic model for turbulent flow over undulating topography and progressive waves. Ph.D thesis, Scripps Institution of Oceanography, University of California, San Diego, 91 pp.